On How Structural Model Variability Influences Transonic Aeroelastic Stability

S.Marques*, K.J. Badcock†, H.H. Khodaparast‡and J.E.Mottershead§

School of Engineering,

University of Liverpool,

L69 3BX, United Kingdom.

This paper considers the ways in which structural model parameter variability can influence aeroelastic stability. Previous work on formulating the stability calculation (with the Euler equations providing the aerodynamic predictions) is exploited to use Monte Carlo, Interval and Perturbation calculations to allow this question to be investigated. Three routes are identified. The first involves variable normal mode frequencies only. The second involves normal mode frequencies and mode shapes. Finally, the third, in addition to normal mode frequencies and mode shapes, also includes their influence on the static equilibrium. Previous work has suggested only considering route 1, which allows significant gains in computational efficiency if reduced order models can be built for the aerodynamics. However, results in the current paper show that neglecting route 2 can give misleading results for the flutter onset prediction.

I. NOMENCLATURE

Symbols

A	**Jacobian matrix**
E	**Residual vector of nonlinear eigenvalue problem**
p	**eigenvector**
R	**Residual vector of the fluid and/or structural model**
S	**Schur complement matrix**
w	**vector of fluid and/or structural unknowns**

Greek

λ	**eigenvalue**
μ	**Bifurcation parameter (altitude)**
ϕ	**normal mode shape**
θ	**Vector containing the uncertain structural parameters**
ω	**normal mode frequency**

Subscripts or superscripts

f	**fluid model**
s	**structural model**
0	**equilibrium**
$\overline{\theta}$	**the vector θ evaluated at the mean structural parameters**

*Research Associate, MAIAA

†Professor, SMAIAA, corresponding author. Tel. : +44(0)151 794 4847 , Fax. : +44(0)151 794 6841, Email : K.J.Badcock@liverpool.ac.uk

‡Research Associate

§Professor

e	solution vector of the eigenvalue problem
s	series approximation

II. Introduction

For in-service aircraft, structural variability arises from several sources, such as manufacturing tolerances, material differences and wear. A study of the McDonnell Douglas F-4 Phantom II[1] quantified the weight and inertia variability for this aircraft, showing changes in mass and inertias of control surfaces by up to 15%. Simulations which are used to characterise the aeroelastic stability of an aircraft need to identify the consequences of the variability or uncertainty in model parameters. A review of this subject was given in reference.[2] Propagation methods for calculating the non-deterministic bifurcation point include Monte Carlo simulation, the perturbation method, polynomial chaos expansions and interval analysis. Whichever method is used, there is a significant implication for increased computational cost when compared with single deterministic calculations. In addition, the numerical statement of the flutter point uncertainty is unlikely in itself to be sufficient, even in the form of a probability distribution or interval. The physical mechanisms underlying the distribution/interval are also required to allow decisions to be based on the predictions. The interpretation in this way is not routinely presented in published research studies.

For transonic aeroelasticity, for fully convincing analysis, there is a requirement to use an aerodynamic simulation based on the nonlinear potential, Euler or Navier-Stokes equations. This brings a very severe implication for the computational cost of non-deterministic analysis. In consequence there has been much interest in reduced order models for this purpose. In reference[3] where a reduced model was created based on mean parameter mode shapes. This model was then used at low cost for the non-deterministic analysis. There is a strong practical reason for adopting this approach. However, it is not evident whether a reduced order model for the aerodynamics built in this way can account for all of the important ways in which the structural parameter variability can impact on the aeroelastic problem. This is the main topic of this paper.

Progress has been made in the development of fast (relative to time domain analysis), Euler based eigenvalue flutter stability prediction methods.[4] The approach, based on an eigenvalue solution of a coupled CFD-FEM system, reduced the cost of non-deterministic flutter calculations at transonic conditions.[5] As part of an effort to evaluate the influence of structural variability, stochastic tools to evaluate the effects of structural variability have been coupled with this eigenvalue method.[5] The perturbation method produces a probability density function (PDF) that allows estimation of flutter uncertainty, assuming a small variation in the input parameters. An alternative approach is interval analysis, that requires defined bounds for the variation of the uncertain parameters. An optimisation procedure finds the worst possible combination, with respect to flutter, of the input parameters. Finally, Monte Carlo simulation provides a relatively expensive option to characterise the PDF accurately. In each case the eigenvalue stability method has been configured to allow the large amount of computation to be done at a feasible cost.

A recent study[6] investigated three routes for the influence of the structural variability on the aeroelastic response: the influence of the distribution of normal mode frequencies; the effect of changing the mode shapes together with the frequencies; the influence of variability of the structural parameters on the aerostatic solution. It was concluded that for some cases, the source of the flutter uncertainty is mainly restricted to normal mode frequency effects. This paper aims to complete this study, by examining test cases of increasing complexity. A systematic approach is proposed that evaluates the routes of influence for structural variability and the effects on flutter uncertainty.

The paper continues with a brief summary of the aerodynamic, structural and eigenvalue stability formulation. A notation for discussing the routes for variability influence is then given. Then results are presented for the Goland wing, a transport wing and a generic fighter, and are used to consider the importance of the routes. Finally, conclusions are drawn.

III. Formulation

A. Aeroelastic Stability

The semi-discrete form of the coupled CFD-FEM system is written as

$$\frac{d\mathbf{w}}{dt} = \mathbf{R}(\mathbf{w}, \mu) \tag{1}$$

where

$$\mathbf{w} = [\mathbf{w}_f, \mathbf{w}_s]^T \tag{2}$$

is a vector containing the fluid unknowns ($\mathbf{w}_f$) and the structural unknowns ($\mathbf{w}_s$), and

$$\mathbf{R} = [\mathbf{R}_f, \mathbf{R}_s]^T \tag{3}$$

is a vector containing the fluid residual ($\mathbf{R}_f$) and the structural residual ($\mathbf{R}_s$). In the current work the structure is modelled by a small number of modes. The residual also depends on a parameter μ (in this paper μ is altitude) which is independent of w. An equilibrium $\mathbf{w}_0(\mu)$ of this system satisfies $\mathbf{R}(\mathbf{w}_0, \mu) = \mathbf{0}$.

The stability of equilibria of Eq. (1) is determined by eigenvalues of the Jacobian matrix $A = \partial\mathbf{R}/\partial\mathbf{w}$. The details of the Jacobian calculation are given in references.[7,8] Write the coupled system eigenvalue problem as

$$\begin{bmatrix} A_{ff} & A_{fs} \\ A_{sf} & A_{ss} \end{bmatrix} \mathbf{p} = \lambda \mathbf{p} \tag{4}$$

where p and λ are the complex eigenvector and eigenvalue respectively. Partition the eigenvector as

$$\mathbf{p} = [\mathbf{p}_f, \mathbf{p}_s].^T \tag{5}$$

The eigenvalue λ satisfies[9] the nonlinear eigenvalue problem

$$S(\lambda)\mathbf{p}_s = \lambda \mathbf{p}_s \tag{6}$$

where $S(\lambda) = A_{ss} - A_{sf}(A_{ff} - \lambda I)^{-1} A_{fs}$. The solution of this problem is discussed in reference,[4] and is based on an approximation to the matrix $(A_{ff} - \lambda I)^{-1}$ given by

$$(A_{ff} - \lambda I)^{-1} = A_{ff}^{-1} + \lambda A_{ff}^{-1} A_{ff}^{-1} + ... \tag{7}$$

This series converges for small values of λ, and so in practice a shift is used to ensure this condition. The details of how to define the shift are described in reference.[4]

There are a number of dependencies and options for this nonlinear eigenvalue problem that are relevant in this work. Define the residual of the eigenvalue problem given by Eq. (6) as

$$\mathbf{E}(\mathbf{w}_0, \lambda, \mathbf{p}_s, \phi, \omega) = (A_{ss} - A_{sf}(A_{ff} - \lambda I)^{-1} A_{fs})\mathbf{p}_s - \lambda \mathbf{p}_s. \tag{8}$$

Note the dependence of this residual on the static solution $\mathbf{w}_0$ through the Jacobian matrices A_{ff}, A_{sf} and A_{fs} which are all evaluated at the static solution. This residual depends on the structural normal mode shapes ϕ through the matrices A_{ss}, A_{sf} and A_{fs}, and the structural normal mode frequencies ω through the matrix A_{ss}. Also, this residual can be computed through one linear solve with the matrix $(A_{ff} - \lambda I)$ against the right hand side $A_{fs}\mathbf{p}_s$, which represents a manageable cost. Write the series approximation to this residual as

$$\mathbf{E}_s(\mathbf{w}_0, \lambda, \mathbf{p}_s, \phi, \omega) = (A_{ss} - A_{sf}(A_{ff}^{-1} + \lambda A_{ff}^{-1} A_{ff}^{-1})A_{fs})\mathbf{p}_s - \lambda \mathbf{p}_s, \tag{9}$$

which, after the pre-computation of the series coefficients, can be evaluated very cheaply. The solution vector for the nonlinear eigenvalue problem is written as $\mathbf{w}_e = [\mathbf{p}_s, \lambda]^T$. Then, two options are available to solve the eigenvalue problem. Both employ Newton's method driven by the Jacobian matrix $\partial\mathbf{E}_s/\partial\mathbf{w}_e$ which can be evaluated rapidly. The first uses the residual E and the second option uses the approximate residual $\mathbf{E}_s$. It was shown in reference[4] that the approximate residual can give good results at the cost of the initial precomputation of the series coefficients.

B. Structural Variability

The approach taken to evaluate the influence on aeroelastic stability follows reference[5]and is summarised here. We assume that the values of some structural parameters θ are uncertain, defined either through a probability density function or by an interval of equally possible values. In either case we can define a mean or midpoint value. The building block for the propagation of the uncertainty in the structural parameters to the uncertainty in the aeroelastic eigenvalues is the ability to evaluate the eigenvalue at low cost for any desired value of the parameter vector θ. This is done in the following way. The matrices for the series approximation in Eq. (7) are first evaluated at the mean or midpoint value for θ. This series approximation is then used to drive the Newton convergence to the aeroelastic eigenvalues for any mode set derived from the required value of θ. The residual E must be evaluated using the full evaluation since the series approximation is only valid for the mean or midpoint structural parameters. In this way the aeroelastic eigenvalue for a modified mode set can be obtained in a small number of additional linear solves once the mean parameter series approximation to S is calculated. This approach is at the heart of the propagation methods used.

The interval analysis requires definition of a range for the uncertain structural parameters, and then computes the possible range for the aeroelastic eigenvalues. A range for each of the important structural parameters is chosen, and then an optimisation problem must be solved to find the range on the critical eigenvalue. A minimisation function in Matlab (*fmincon*), that solves a constrained non-linear multivariate problem, is used. This method requires the parameter constraints (i.e. intervals) and a scalar objective function.

C. Variability Routes

For two reasons the way that the variability in structural parameters influences the flutter stability needs to be understood. First, this understanding can possibly lead to improved propagation methods. More fundamentally, without this insight the meaning of the results of the analysis is not clear. To allow a systematic investigation of this problem three ways, or routes, for influence are defined as

1. Normal mode frequency - the variability changes the normal mode frequencies
2. Normal mode shape - the variability changes the normal mode shapes
3. Static equilibrium - the change of normal mode shapes and frequencies changes the static equilibrium.

In the notation already introduced the following scenarios can be considered by applying the approach for treating structural variability in different ways:

- Route 1 can be computed by solving the nonlinear eigenvalue problem defined by the residual $\mathbf{E}_s(\bar{\mathbf{w}}_0, \lambda, \mathbf{p}_s, \bar{\phi}, \omega)$. The series residual is evaluated with the normal mode frequency regarded as dependent on the variable structural parameters, but at the mean structural parameter normal modes (denoted $\bar{\phi}$), and the equilibrium calculated at the mean normal modes and frequencies, denoted $\bar{\mathbf{w}}_0$.
- Routes 1 and 2 combined can be computed by solving the nonlinear eigenvalue problem defined by the residual $\mathbf{E}(\bar{\mathbf{w}}_0, \lambda, \mathbf{p}_s, \phi, \omega)$. This was the problem solved in reference,[5] and used the mean parameter equilibrium, and with both the normal mode frequencies and mode shapes dependent on the variable structural parameters.
- Routes 1-3 can be combined by solving the nonlinear eigenvalue problem defined by the residual $\mathbf{E}(\mathbf{w}_0, \lambda, \mathbf{p}_s, \phi, \omega)$. In this case the equilibrium is also considered dependent on the normal mode frequency and shapes which depend on the variable structural parameters.

From a computational perspective, route 1 is by the far the cheapest to compute. In previous work[3] a reduced model was computed for the mean structural parameter mode set, i.e. only accounting for route 1, and was used to study the effects of structural uncertainty on flutter. However, it has also been pointed out[20] that some reduced models require further information on the modified structural models, i.e. using routes 2 and 3. Therefore it is of practical interest to understand when routes 2 and 3 are important.

IV. Results

A. Goland Wing

The Goland wing, shown in Fig. 1(a), has a chord of 1.8m and a span of 6m. It is a rectangular cantilevered wing with a 4% thick parabolic section. The structural model follows the description given in reference.[10] The CFD grid is block structured and uses an O-O topology. The fine grid has 250 thousand points and a coarse level was extracted from this grid, which has 40 thousand points. Grid refinement results reported previously in reference[4] showed that the coarse grid gives accurate aeroelastic damping predictions. Four mode shapes were retained for the aeroelastic simulation, the first and second bending and torsion modes.

The case we consider here has a mass added to the wing tip to represent the presence of a tip store. The baseline position is 7.5cm from the leading edge. The store is offset 52.5cm from the elastic axis, (*ea*), and has a total mass of 328.3kg, which represents 1/10 of the total wing mass (corresponding to the mass of one rib). The baseline location is indicated in Fig. 1(b). For the baseline case the flutter boundary is shown in Fig 1(c) and shows that stability is rapidly lost at a Mach number of 0.92. This is due to the strengthening of a shock wave located towards the trailing edge, shown at this Mach number in figure 1(d).

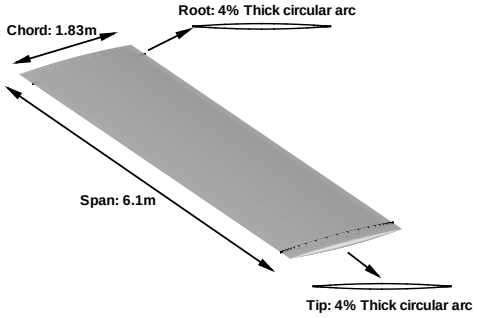

(a) Geometry

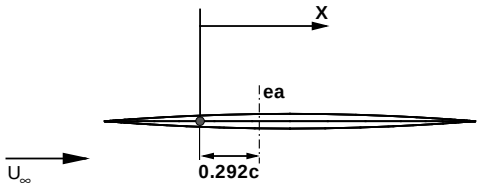

(b) Schematic of Store Mass Location

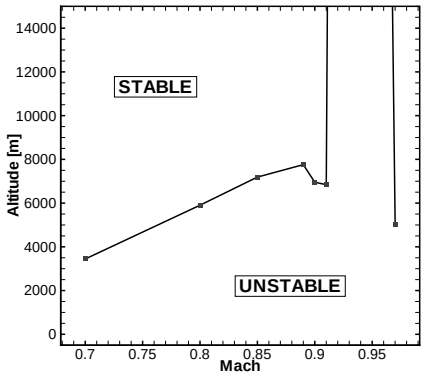

(c) Flutter Boundary - Baseline Case

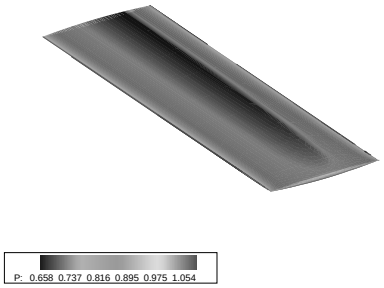

(d) Surface Pressure Distribution

Figure 1. Goland Wing$^+$. In part (c), flutter boundary for baseline store mass location; for part (d), M=0.92, $\alpha = 0^\circ$

The case selected for studying variability was at Mach 0.91 and zero degrees incidence, close to where stability is rapidly lost with increasing Mach number. The store mass location is regarded as the uncertain parameter. Note that the wing is symmetric and the angle of attack is zero and so the static solution is independent of the store mass location, and hence only variability routes 1 and 2 are relevant for this case.

The mean parameter modal interaction is shown as a function of altitude in Fig. 2(a) and

(b). Stability is lost at 7200m, with modes 3 and 4 (second torsion and bending respectively) interacting and mode 3 going undamped. Note that modes 1 and 2 (first bending and torsion respectively) are also interacting strongly, with mode 1 going undamped at a lower altitude. The variation with the store mass location of the real part of the four aeroelastic eigenvalues at an altitude of 9000m (just above the flutter value for the baseline case) is shown in Fig. 2(c) and (d). As the store mass is moved aft the damping of modes 3 and 4 is insensitive. However, the damping of mode 1 is rapidly lost.

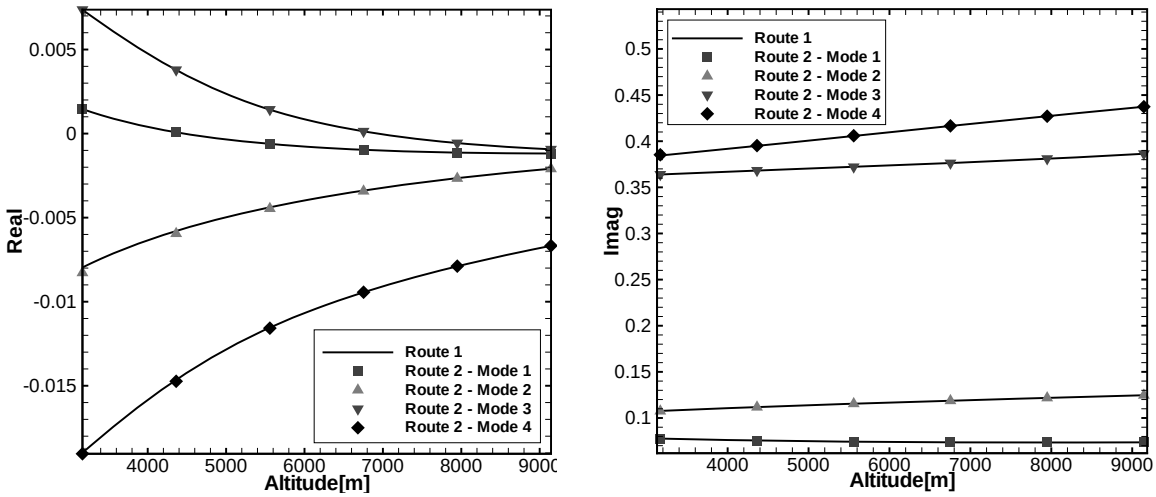

(a) Baseline Store Location

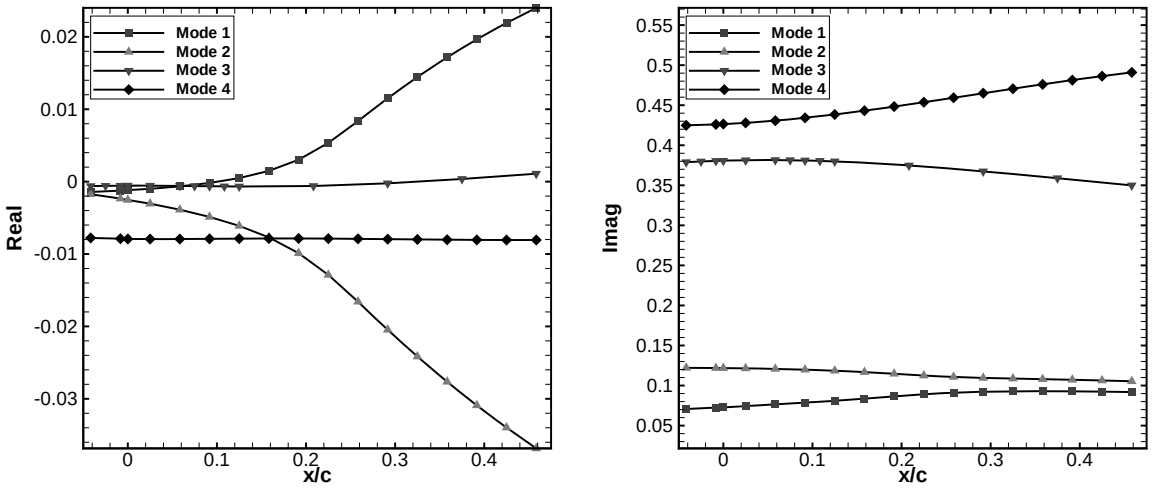

(c) Real part variation

(d) Imaginary part variation

Figure 2. Goland Wing$^+$, M0.91, $\alpha = 0°$; parts (a) and (b) - variation with altitude for baseline store mass location; parts (c) and (d) - variation with store mass location at an altitude of 9000m

A variability analysis was next carried out to examine the importance of the different routes of influence. A normal distribution was assumed for the store location, with the mean at the baseline location and a coefficient of variations of 2.8%. Finite differences were used to compute the derivative of the real part of the aeroelastic eigenvalues with the store mass location, and these values are shown in Fig. 3(a). The derivatives were calculated assuming routes 1 and 2, and the parameter and real part values are normalised with their mean values in the derivative calculation. Recall that route 1 includes the influence of the store mass location on the normal mode frequencies only, and that route 2 includes the influence on normal mode frequencies and mode shapes. It is seen that the sign of the derivative for mode 1 (i.e. whether the predicted damping increases or decreases) is different with the two assumptions. In this case the exact values are for route 2 since there is no dependence of the steady state on the store location, as commented above. Hence, the

route 1 results are misleading. This is further illustrated in Fig. 3(b) where a histogram of the real part is shown. The histogram was formed by counting the number of values falling within equally spaced intervals. Note that the distributions are not very different for routes 1 and 2. However, if the values from the two routes are cross-plotted, as shown in Fig. 3(c), the perturbation results are confirmed as it is clear that the relationship has a negative slope. If the predictions of the two routes are in perfect agreement then this graph will result in a line of slope 1. Hence the agreement of the histograms is fortuitous.

To explain the differences between route 1 and 2 predictions the influence of the store mass location on the normal modes was characterised by plotting the variation of the normal mode frequencies and mode shapes with the store mass location. The frequency variation is shown in Fig. 3(d) in terms of the change from the mean parameter values. The mode shapes are characterised by the leading edge tip bending and tip torsion, and are again plotted in terms of the change from mean parameter values in Figs. 3(e) and (f) respectively.

For the route 1 perturbation result, the damping of mode 1 increases with the aft movement of the store. Mode 1 is interacting with mode 2. Looking to the behaviour of the normal mode frequencies with the aft movement of the store, the frequency for mode 1 is insensitive, but the frequency of mode 2 is increasing, meaning that the difference in frequencies between modes 1 and 2 is increasing. This leads to an increased damping of the first aeroelastic mode, as indicated by the perturbation analysis.

The route 2 results also include the change of mode shapes with changing store location. The modes interacting are the first bending and torsion modes, and an aft movement of the store mass moves the centre of gravity aft which tends to make the system more unstable, taking a two dimensional pitch-plunge aerofoil system as a guide.[11]

B. MDO Wing

The MDO wing is a commercial transport wing, with a span of 36 metres, designed to fly in the transonic regime.[12,13] The profile is a thick supercritical section. The geometry is summarised in figure 4. The structure is modelled as a wing box running down the central portion of the wing. The problems of mapping this reduced planform to the full planform CFD model are considered in reference.[14] The CFD grid used has 81 thousand points. Results generated using the inverse power method to track eigenvalues were previously shown.[15] The eigenvalue formulation used in this paper was applied to the MDO wing in reference.[4] In the current work seven modes are retained and the mapped modes which particate in the aeroelastic instability are shown in Fig. 5.

Here we consider the case with a freestream Mach number of 0.85 and an angle of attack of 1 degree. The wing density, Young's modulus and Shear modulus are considered uncertain. The aeroelastic eigenvalues of the original model were traced with altitude and are shown in Fig. 6. Note that in this case the steady state does depend on altitude and so all three routes are potentially relevant for the influence of uncertainty. The aerostatic deflection moves the tip up and twists it nose down which initially has the effect of alleviating the shock wave. This has the effect of moving the altitude where instability is encountered to a lower value compared with the jig shape. The lines on the figure for the mode tracking are based on the series solution and so jump when the aerostatic solution (and subsequently the Schur matrix) is updated. The symbols always represent the nonlinear solution for the correct aerostatic solution at each altitude. Modes 1, 2 and 4 participate in the aeroelastic instability mechanism, with stability lost in mode 1 at around 4750m.

Variability results are shown for mode 1 which goes unstable first for the mean structural parameters. Again normal distributions were assumed for the density, Young's modulus and Shear modulus, with mean values of **2700** kg/m^3, **7.1** $\times 10^{10} N/m^2$ and **2.7** $\times 10^{10} N/m^2$ respectively. A coefficient of variation of 2.5% was used in each case. Routes 1,2 and 3 are now considered. The derivatives of the real part of the first mode eigenvalue are shown in Fig. 7(a) with respect to the three structural parameters considered. The derivative with respect to density is positive in all three cases (indicating that the wing becomes less damped as the density increases), whereas it becomes more damped with increasing Young's and Shear modulus. Considering the different routes leads to most difference in the values from the density, where route 1 gives the largest value, route 2 a significant reduction, and additionally route 3 a further small reduction.

The histograms based on 250 samples are shown in Fig 7(b) and (c) for the Young's modulus and density variations respectively. These results are consistent with the sensi-

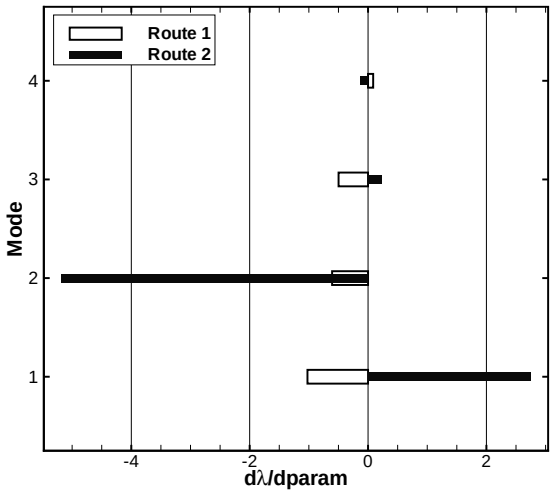

(a) Derivatives at Baseline Location

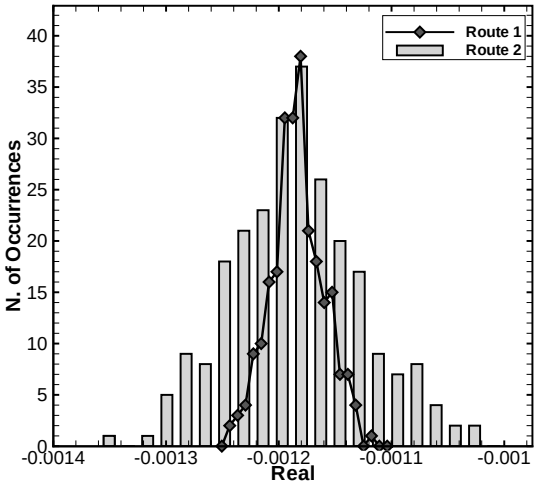

(b) Histogram for mode 1 real part

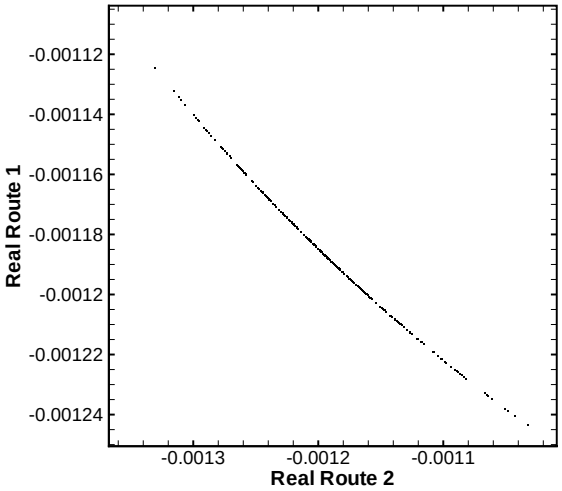

(c) Routes 1 and 2 correlation for mode 1 real part

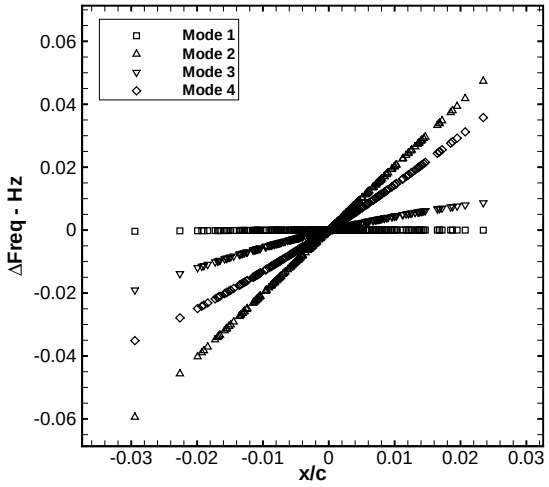

(d) Normal Mode Frequency Variation

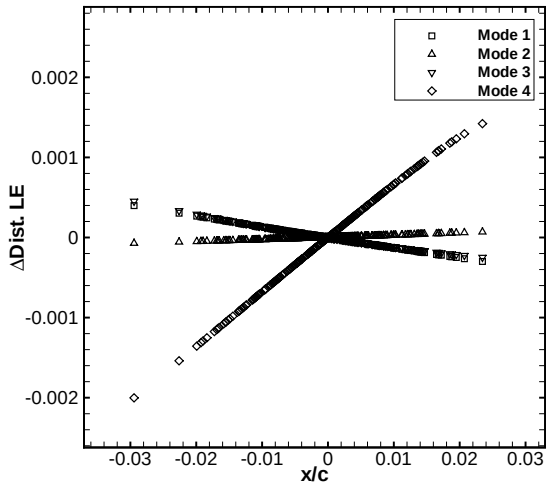

(e) Normal Mode Tip Deflection Variation

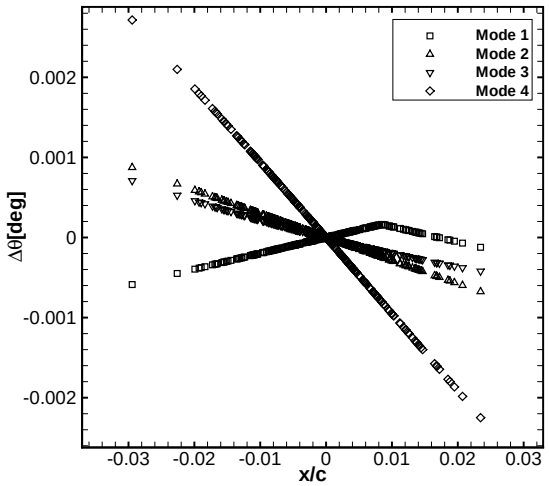

(f) Normal Mode Tip Torsion Change

Figure 3. Goland Wing$^+$, M0.91, $\alpha = 0°$ at an altitude of 9000m

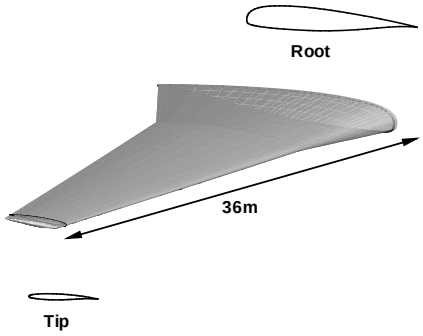

Figure 4. MDO Wing model.

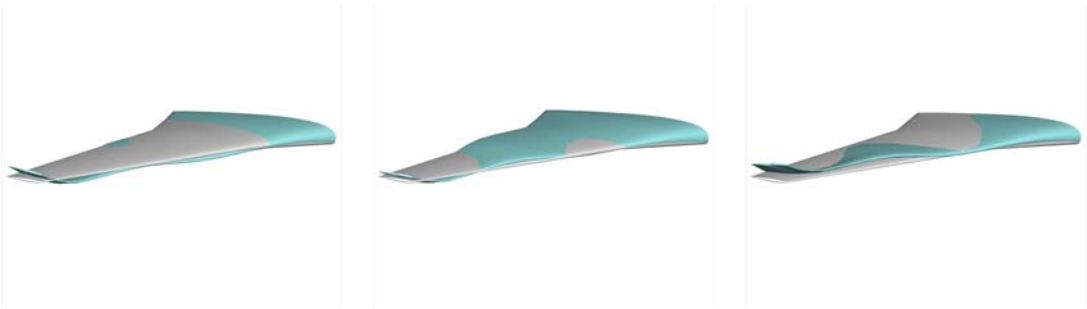

(a) Mode 1 - 0.8440 Hz (b) Mode 2 - 2.162 Hz (c) Mode 4 - 3.989 Hz

Figure 5. MDO mode shapes

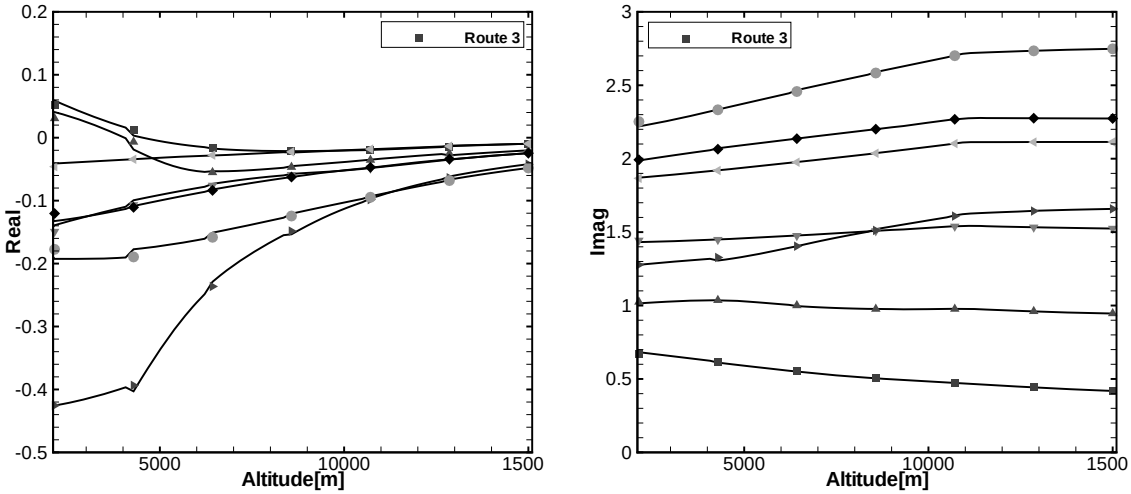

(a) Real Part (b) Imaginary Part

Figure 6. Mode tracking - MDO Wing, M=0.85, $\alpha = 1^\circ$

tivity results. For Young's modulus the standard deviation is similar in all three cases. For the density variation the level 1 histogram has the largest spread, with the route 3 case having very little variation at all about the mean value.

To interpet this behaviour the normal mode variation with the parameters was again characterised using the change from mean parameter values for the frequency, tip leading edge bending and tip section torsion. These are shown in Fig 8. For increasing density the normal mode frequencies of the participating modes move together, leading to an increasing real part for mode 1. In contrast, for increasing Young's modulus the frequencies move apart, leading to a more negative real part. The tip bending decreases and the tip section torsion increases for increasing density. The increasing torsion appears to promote a more unstable situation. The tip bending of modes 1 and 2 decreases with increasing Young's modulus, and the tip section torsion decreases for all three modes. The influence of these variations is to reduce the real part of the mode 1 aeroelastic eigenvalue, i.e. to make the wing more stable.

Finally, the route 3 influence is strongest for the density. In this case increasing the density will reduce the aerostatic deflection. At the altitude used for this analysis the wing tip is already twisted to a nose down location (shown in Fig. 9), meaning that a reduced static deflection results in a less negative effective angle of attack. This leads to more damping with increased density at this altitude, and this is in agreement with the perturbation result which has a less positive value from route 3 compared with route 2.

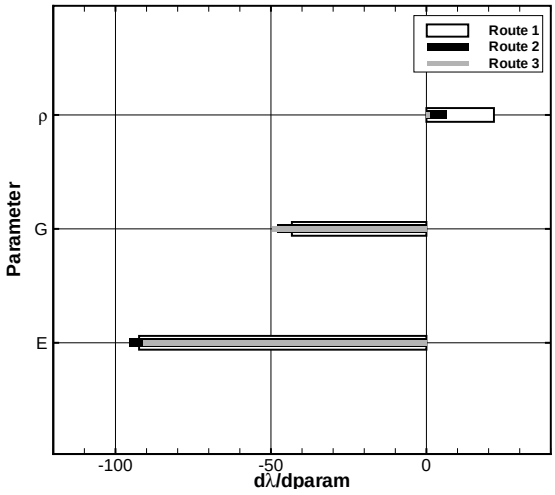

(a) Mode 1 real part sensitivity

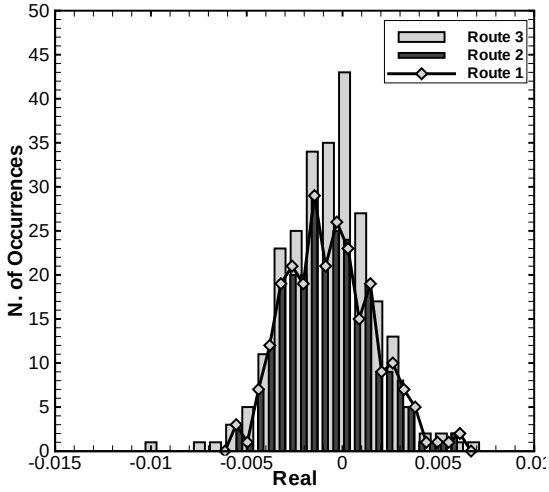

(b)Varying Young's Modulus

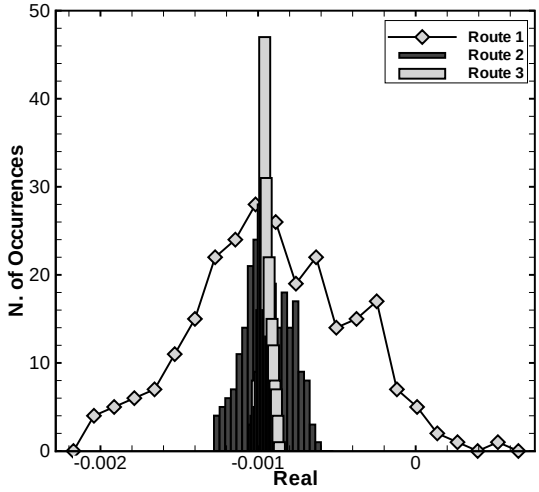

(c) Varying Material Density

Figure 7. Mode tracking - MDO Wing, M=0.85, $\alpha = 1^\circ$

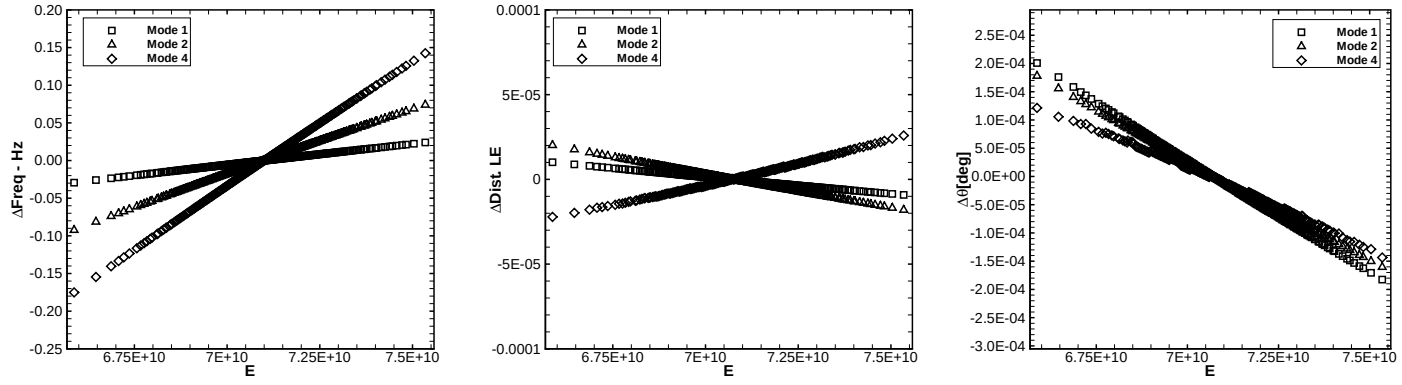

(a) Young's modulus

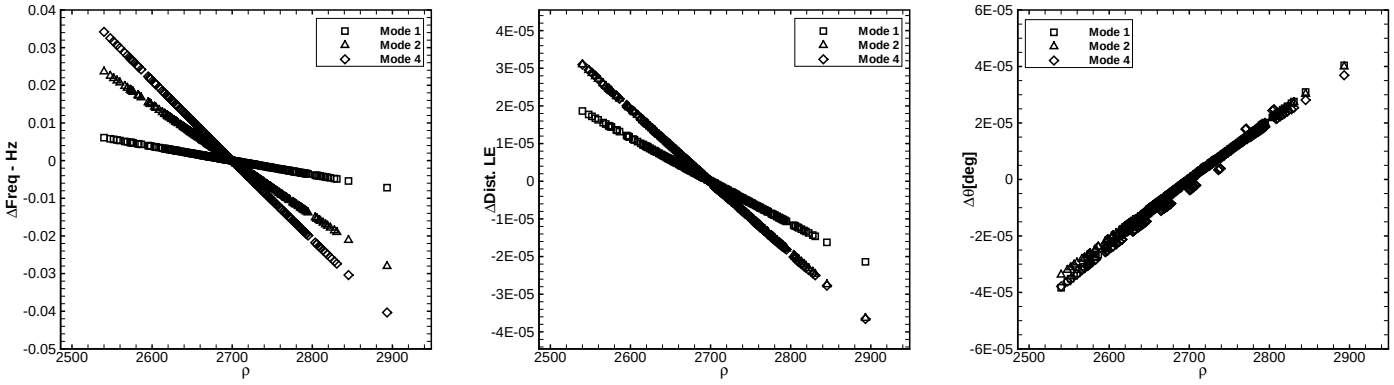

(b) Material Density

Figure 8. Variation due to structural parameter variability - MDO Wing, M=0.85, $\alpha = 1^\circ$ - 250 samples

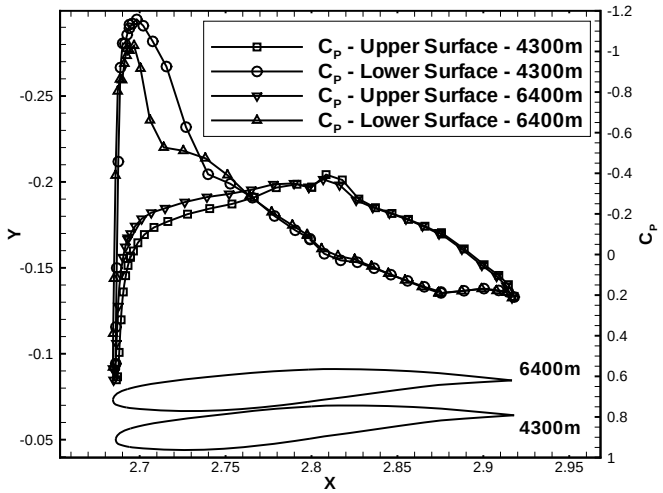

Figure 9. Static tip deformation and cp distribution, M=0.85, $\alpha = 1^\circ$

C. Generic Fighter

Finally a realistically sized aircraft model is considered. The open source fighter was built on data publically available for the F-16 aircraft[a]. The approach was to establish a test case with aeroelastic behaviour representative of an aircraft. Available data for the wing geometry (dimensions and aerofoil section), together with published data from Ground Vibration Tests (GVT) and wind-tunnel data was used.

The geometry is summarised in Fig. 10 and was described in reference.[5] The aerofoil section consists of a NACA 64A204 profile, with a wing root angle of -1° and a wing tip angle of -2.4°. The twist was chosen by comparing with published surface pressures for the F-16. A coarse grid was generated with 1.06 million points and 344 blocks for the full configuration. This was extracted from a fine grid with 8.5 million points for the full configuration which was used in reference[5] to demonstrate grid convergence on the coarse grid.

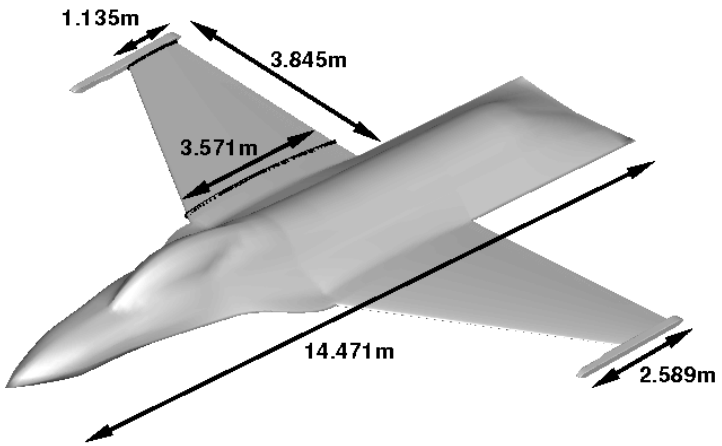

Figure 10. Open Source Fighter geometry.

The finite-element (FE) model of the wing was built in NASTRAN based on the model proposed by Cattarius.[16] The structural model consists of four parts: fuselage, wing, pylon and stores. The fuselage, pylon and stores are considered to be effectively rigid. The mass properties of the pylon and stores are represented by lumped masses. The pylon is rigidly connected to the wing. The store is connected to the pylon by six spring elements (three translational and three rotational). The wing is also modelled using shell elements and is divided into three regions: root, pylon, and tip. In order to match the natural frequencies of the FE model to those found in the Ground Vibration Test,[17] the Young's modulus and density of each region of the wing are considered as updating parameters. Fig. 11 shows the mode shapes of the full model which participate in the aeroelastic mechanism. The

[a]Files defining the model are available at www.cfd4aircraft.com

modal frequencies are compared with tests in reference[5] and show good agreement with the available data (which is for the symmetric modes). The mapping between the CFD and FEM grids was done using the transformation method described in reference.[19] The two wings are connected by a plate in the structural model, and this plate is used to drive the aerodynamic grid on the fuselage.

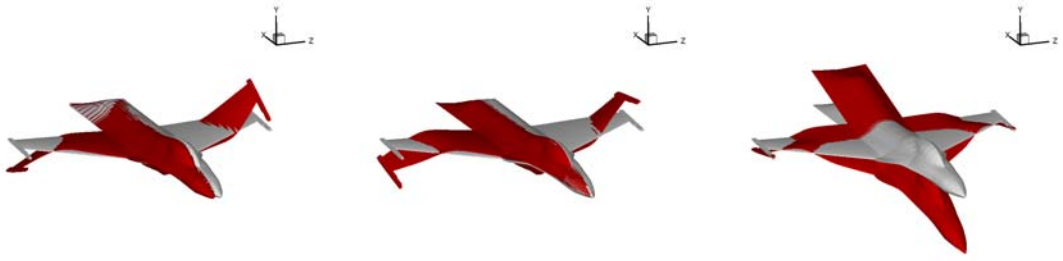

(a) Mode 2 - 4.48Hz (b) Mode 3 - 5.03Hz (c) Mode 4 - 5.92Hz

Figure 11. Selected Mapped Structural Normal Modes for the Open Source Fighter.

Previous work using linear analysis[18] and the Euler equations[5] identified by perturbation analysis the critical structural parameters for determining the flutter point. These were found to be the rotational spring coefficient for the store attachment (mean value $2000kNm/rad$), the Young's modulus of the wing root section ($1.573 \times 10^{11} N/m^2$) and the pylon ($9.67 \times 10^{10} N/m^2$), and the densities for the wing root ($5680kg/m^3$) and tip ($3780kg/m^3$) regions, and the pylon ($3780kg/m^3$). A coefficient of variation of 1.5% was used for all variables. The conditions used for analysis in these papers was a Mach number of 0.85 and zero degrees incidence, and these are used again in this paper. Mean values used were The mean parameter aeroelastic mode tracking at these conditions is shown in Fig. 12. The antisymmetric modes 2 (torsion) and 3 (bending) interact, with the third mode becoming undamped at 1969 m.

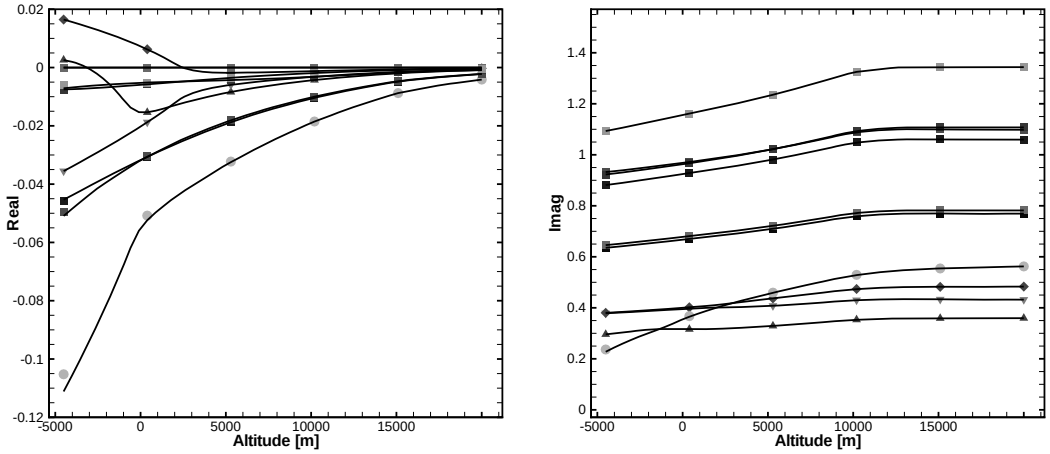

(a) Real (b) Imaginary

Figure 12. Mode tracking - Generic Fighter, M0.85, $\alpha = 0^\circ$

The variability results are shown in Fig 13. At mean parameter values it is mode three (antisymmetric bending) that goes undamped, and the sensitivity of the real part of this mode is shown in Fig 13(a) for the six most important structural parameters. The mid-wing Young's modulus, wing root density and the store attachment rotational stiffness are the most important values, and it is seen that the signs of the derivatives for the first two of these are the same between the route 1 and 2 cases, but for the spring attachment there is a big discrepancy in the two cases.

Next, the histograms from a Monte-Carlo simulation for routes 1 and 2 are shown in Fig

13(b) and (c), with all 6 parameters varying in the first case, and only the wing root density in the second case. It is seen in both cases that the route 2 results show a larger spread. The six parameter results also show a larger spread than the density only results. These results are consistent with the perturbation results in that the most significant derivatives for route 2 are all larger in magnitude than for route 1, and the Young's modulus derivatives are the largest of all once normalised. The correlation between the route 1 and 2 real parts is plotted in Fig 13(d) and (e), and shows that they correspond reasonably well. In this case the route 1 results are a reasonably good guide to the variability in the eigenvalue.

Characterising the impact of the wing root density on the normal modes, the frequency and mode shape variations are shown in Fig. 14. As the root density increases the modal frequencies increase in order for the interacting modes, with higher frequencies increasing more. This leads to the damping of these modes increasing, and in particular the real part of the aeroelastic eigenvalue of mode 3 decreases, as predicted by the perturbation analysis. The bending at the leading edge wing tip decreases for modes 2 and 4 with increasing root density, but increases for the antisymmetric bending mode 3. Finally, the tip torsion increases for mode 2 (antisymmetric torsion) and decreases for the other two modes. It is difficult to interpret why this leads to the more stable aeroelastic interaction which is indicated by the perturbation results.

V. Conclusions

An aeroelastic stability calculation method based on aerodynamics from the Euler equations and an eigenvalue calculation was used to investigate the ways that structural parameter variation can influence stability. A systematic approach was afforded by the formulation, to allow the three possibles routes of influence to be isolated. Three test cases were used to evaluate the influences.

Considering the first route only, which is the influence of the variation on the normal mode frequencies, allows for the aerodynamic effects to be computed for mean parameter modes shapes only. This dramatically enhances the efficiency of the non-deterministic calculations. For the Goland wing case this assumption predicted the wrong trend, for the MDO case the variation with density was significantly overpredicted and for the Open Source Fighter the variation was overpredicted. It was therefore seen that it is not generally the case that this approach is adequate.

The second route includes the influence of structural parameter variability on the modes shapes as well. This provides the exact answer for the Goland wing case. For the MDO case the third route was also considered, namely the influence of the variation on the aerostatic solution. This was found to signifiantly reduce the variation in stability with respect to the material density.

It is therefore concluded that all three routes should be considered for a variability analysis, and that this means that aerodynamic reduced models must be capable of describing the influence of all three routes. This has unfortunate computational cost implications. Perturbation analysis can however give good information about what when the more expensive analyses are needed.

VI. Acknowledgements

This work is funded by the European Union for the Marie Curie Excellence Team ECERTA under contract MEXT-CT-2006 042383.

References

[1]Pitt, D., Haudrich, P. and Thomas, M., "Probabilistic Aeroelastic Analysis and Its Implications on Flutter Margin Requirements", AIAA Paper 2008-2198, 2008.

[2]Pettit, C., "Uncertainty Quantification in Aeroelasticity: Recent Results and Research Challenges", *Journal of Aircraft*, Vol. 41, No 5, 2004, pp. 1217-1229.

[3]Wang, Z., Zhang, Z., Lee, D. H., Chen, P. C. and Liu, D. D., "Flutter Analysis with Structural Uncertainty by Using CFD-based Aerodynamic ROM', AIAA 2008-2197, 2008.

[4]Badcock, K.J. and Woodgate, M.A., "Prediction of Bifurcation Onset of Large Order Aeroelastic Models", AIAA Paper 2008-1820, 2008.

[5]Marques, S., Badcock, K.J., Khodaparast, H.H. and Mottershead, J.E., "CFD Based Aeroelastic Stability Predictions Under the Influence of Structural Variability', *Journal of Aircraft*, to

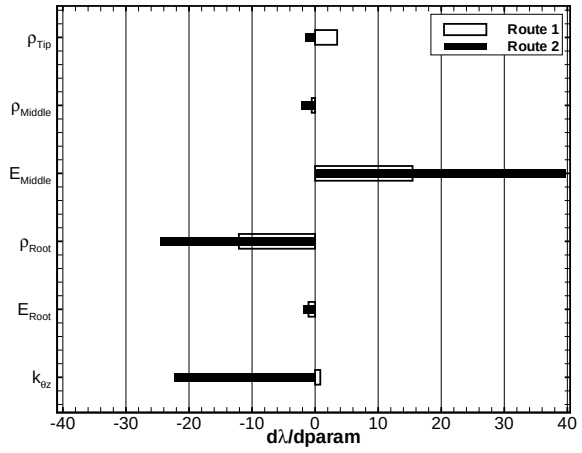

(a) Normalised Sensitivity

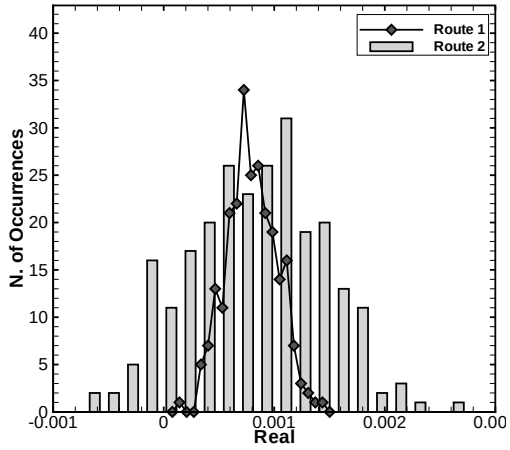

(b) Mode 3 Histogram with variability on 6 parameters

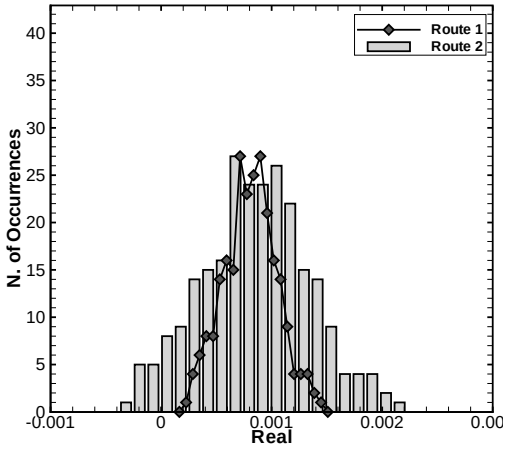

(c) Mode 3 Histogram with variability on wing root density

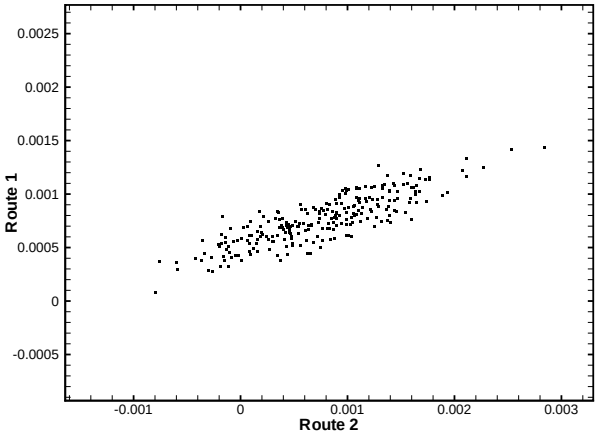

(d) Mode 3, routes 1 and 2 six parameters correlation

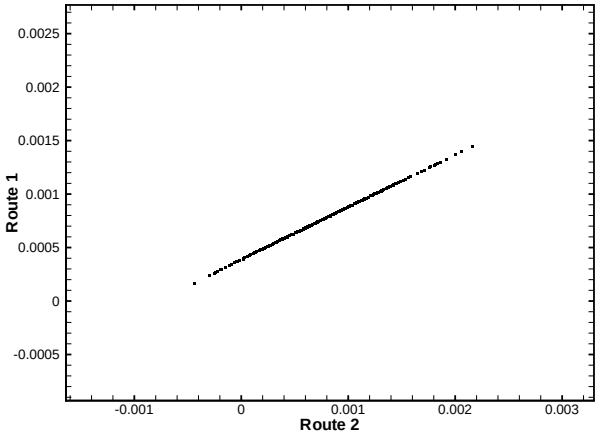

(e) Mode 3, routes 1 and 2 correlation for wing root density

Figure 13. Variability analysis at Mach 0.85, zero degrees incidence.

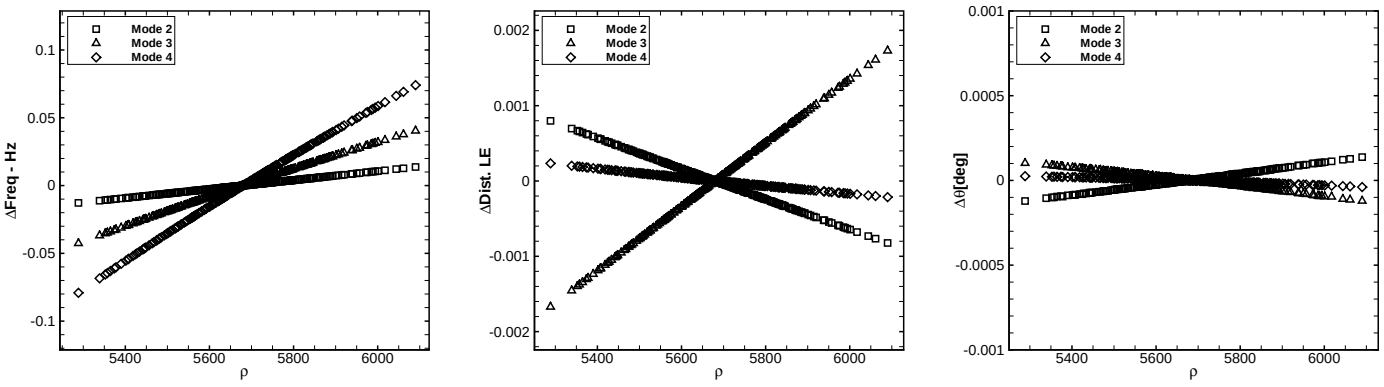

Figure 14. Normalised Real Eigenvalue parameter sensibility, M-16, M=0.85, $\alpha = 0°$

appear, 2010.

[6]Marques, S., Badcock, K.J., Khodaparast, H.H. and Mottershead, J.E., "Evaluation of the Impact of Structural Model Variability on Transonic Aeroelasticity", IFASD-2009-063 in the proceedings of International Forum on Aeroelasticity and Structural Dynamics, Seattle, Washington, 2009.

[7]Badcock, K.J., M.A. Woodgate, M.A. and Richards, B.E., "The Application of Sparse Matrix Techniques for the CFD based Aeroelastic Bifurcation Analysis of a Symmetric Aerofoil", *AIAA Journal*, Vol. 42, No. 5, 2004, pp 883-892.

[8]Badcock, K.J., Woodgate, M.A. and Richards, B.E., 'Direct Aeroelastic Bifurcation Analysis of a Symmetric Wing Based on the Euler Equations', *Journal of Aircraft*, Vol. 42, No. 3,2005, pp. 731-737.

[9]Bekas, K. and Saad, Y., "Computation of Smallest Eigenvalues using Spectral Schur Complements", *SIAM Journal of Scientific Computing*, Vol. 27, No. 2, 2005, pp. 458-481.

[10]Beran, P.S., Knot, N.S., Eastep, F.E., Synder, R.D. and Zweber, J.V., "Numerical Analysis of Store-Induced Limit Cycle Oscillarion", *Journal of Aircraft*, Vol. 41, No 6, 2004, pp. 1315-1326.

[11]Dowell, E.H. (editor), A Modern Course in Aeroelasticity, Kluwer Academic Publishers.

[12]Girodroux-Lavigne, P., Grisval, J. P., Guillemot, S., Henshaw, M., Karlsson, A., Selmin, V., Smith, J., Teupootahiti, E. and Winzell, B., "Comparison of static and dynamic fluid-structure interaction solutions in the case of a highly flexible modern transport aircraft wing", *Aerospace Science and Technology*, 7, 2003, 121-133.

[13]Allen, C.B., Jones, D., Taylor, N.V., Badcock, K.J., Woodgate, M.A., Rampurawala, A.M., Cooper, J.E. and Vio, G.A., "A Comparison of Linear and Nonlinear Flutter Prediction Methods: A Summary of PUMA DARP Aeroelastic Results", *Aeronautical Journal*, Vol. 110, No. 1107, May, 2006, 333-343.

[14]Goura, G.S.L., Badcock, K.J. and Woodgate, M.A., "Extrapolation Effects on Coupled Computational Fluid Dynamics/Computational Structural Dynamics Simulations", *AIAA Journal*, Vol. 41, No. 2, February, 2003, 312-314.

[15]Woodgate, M.A. and Badcock, K.J., "On the fast prediction of Transonic Aeroelastic Stability and Limit Cycles", *AIAA Journal*, Vol. 45, No. 6, 2007, 1370-1381.

[16]Cattarius, J, "Numerical Wing/Store Interaction Analysis of a Parametric F-16 Wing" , PhD Thesis, Virginia Polytechnic Institute and State University, Blacksburg, Virginia, U.S., 1999.

[17]Cazier, F.W. Jr and Keloe, M.W., "Ground Vibration Test on an F-16 airplane with modified decoupler pylons", NASA-TM-87634, NASA, 1986.

[18]Khodaparast,H.H., Mottershead, J.E. and Badcock, K.J., "Propagation of Structural Uncertainty to Linear Aeroelastic Stability", accepted for publication in *Computers and Structures*, 2009.

[19]Woodgate, M.A, Badcock, K.J., Rampurawala, A.M., Richards, B.E., Nardini, D and Henshaw, M.J., "Aeroelastic Calculations for the Hawk Aircraft Using the Euler Equations", *Journal of Aircraft*, Vol. 42, No 4, 2005, pp. 1005-1012.

[20]Thomas, J. P., Dowell, E. H. and Hall, K. C., "Three-Dimensional Transonic Aeroelasticity Using Proper Orthogonal Decomposition-Based Reduced-Order Models", *Journal of Aircraft*, Vol. 40, No 3, 2003, pp. 544-551]